State-selective electron capture in 30- and 100-keV He$^+$ + He collisions

D. L. Guo,[1] X. Ma,[1,*] R. T. Zhang,[1] S. F. Zhang,[1] X. L. Zhu,[1] W. T. Feng,[1] Y. Gao,[1] B. Hai,[1,2] M. Zhang,[1,2]
H. B. Wang,[1,2] and Z. K. Huang[1,2]

[1]*Institute of Modern Physics, Chinese Academy of Sciences, Lanzhou 730000, China*
[2]*University of Chinese Academy of Sciences, Beijing 100049, China*

A combined experimental and theoretical study on single capture in 30- and 100-keV He$^+$ on He collisions was performed. By using a reaction microscope, we obtained the state selective cross sections and the angular-differential cross sections. It was found that the experimental state-selective cross sections were in good agreement with the dynamic screening classical trajectory Monte Carlo calculation for 100-keV He$^+$ incident. The comparisons with various versions of such calculations reveal the roles played by different electron-electron correlation effects. Moreover, a prominent oscillatory structure was observed in the angular-differential cross sections for both projectile energies. With the single capture probability distribution obtained from the classical trajectory Monte Carlo calculation, the oscillation structures can be well explained by atomic-size Fraunhofer-type diffraction.

I. INTRODUCTION

Charge exchange (electron capture) between an energetic ion and a neutral atom is a process where one or several target electrons are captured into the bound state of the projectile. The use of charge-exchange spectroscopy as a diagnostic tool in the large high-temperature Tokamak fusion reactor ITER project is a well-established diagnostic technique [1,2], and a renewed focus is given to state-selective electron-capture processes, since the metastable H*($n = 2$) or D* ($n = 2$) will produce a large photon flux resulting in heating in the facing walls and increasing the danger of the plasma touching the walls and quenching the reaction. Additionally, charge exchange was confirmed to be one of the important x-ray sources in astrophysics such as solar wind and comet x-ray emission [3,4]. On the other hand, charge exchange itself is of fundamental importance to develop the few-body atomic collision model. In view of their importance, considerable attention was given for charge-exchange processes from theoretical as well as experimental aspects [5].

From the experimental point of view, most of early measurements focused on the energy dependence of total absolute cross sections [6–8]; however, only a few studies involving differential cross sections which contain much of the information on the collision dynamics were made. Differential cross sections were rare because the traditional experimental techniques, such as energy-loss spectroscopy [9–11] or optical spectroscopy [12,13], are inadequate to study the collision dynamics at the fully differential level. The development of the innovative experimental technique of the reaction microscope [cold-target recoil-ion-momentum spectroscopy (COLTRIMS) as well] renewed the field. Many experimental studies of electron transfer employing this approach in the past decades provided valuable data for the applied area and the most stringent test for the existing theoretical models [14].

From the theoretical point of view, in the intermediate-impact-energy range, the existing theoretical methods are facing challenges due to the strong coupling of the various reaction channels. In spite of the fact, the atomic-orbital close-coupling (AOCC) and molecular-orbital close-coupling (MOCC) methods have demonstrated their advantages in this energy domain [15–20]. The classical trajectory Monte Carlo method (CTMC) has also provided reasonable description for some of the collision process in this energy range [21–27]. In the early stage of the investigations using the reaction microscope, Dörner *et al.* [23], Mergel *et al.* [25], and Moshammer *et al.* [24] have demonstrated the powerful capabilities of CTMC in the interpretation of the highly differential cross-section data. More recently, Alessi *et al.* [28,29] studied the single-capture process in He^{2+} + He, and He$^+$ + H$_2$ collisions at intermediate impact energies by using the CTMC method, and very good agreements were obtained in the comparisons with their measurements.

For the single-capture process, the differential studies in the past focused on two main aspects: the state-selective cross sections and the angular-differential cross sections. From the state-selective cross sections, the critical data essential in many applied fields [30] can be obtained with sufficient resolution. Many studies involving state-selective measurements have been reported in the past [31,32]. Fischer *et al.* [33] measured state resolved differential cross sections for single capture in 3.15 keV/u Ne^{7+} + He collisions and obtained the spectroscopic information about energy levels in highly charged ions. The state-selective single-electron-capture process involving the optically prepared excited states of targets has also been the subject of a series of experimental and theoretical investigations in the past decades [34–40].

The projectile angular-differential cross sections or the angular distributions imply many physics mechanisms. Schöffler *et al.* [41] measured the angular-differential cross sections for ground-state transfer with very high resolution and found mixed agreement with the four-body distorted-wave models. Knoop *et al.* [42] and van der Poel *et al.* [43] found atomic-size Fraunhofer-type diffraction in single-electron capture in He^{2+} + Na collisions. In a subsequent study of He^{2+} + He collisions Wang *et al.* [44] also observed such phenomena. In fact, not only for single capture but also for more

———————
*x.ma@impcas.ac.cn

complicated process such as transfer ionization, the angular-differential cross sections manifest themselves in exploring the collision dynamics. For instance, the famous Thomas scattering mechanisms was verified by Mergel *et al.* [25,45] in the angular-differential cross sections of transfer ionization process occurring in $p +$ He collisions. Very recently, we reported the state-selective cross sections and revealed the role played by the electron-electron correlation effects in intermediate impact energy $p +$ He collisions [46].

The studies using fully stripped ions as projectiles, such as p [46,47], and He^{2+} [44,47], have been extensively made in the past. Processes involving dressed projectiles therefore deserve special attention. In this work, we performed a combined experimental and theoretical investigation on the single capture at 30- and 100-keV impact energies for $He^+ +$ He collisions. In the past, much attention on this symmetric collision system has focussed on obtaining the total differential cross sections [8,48–54]. The comparison between the theoretical results using the four-body continuum-distorted-wave model and numerous experimental measurements reveal overall good agreement [55]. Bradley *et al.* [48] obtained the cross sections for the dominant ground-state transfer process where the captured electron is in the ground state of the projectile. The process involving the transfer of a target electron to the projectile with the simultaneous excitation of a projectile electron has also received much attention for decades [56,57].

In the present paper, we report on state-selective cross sections and projectile angular-differential cross sections obtained experimentally using the reaction microscope and compared with the theoretical results by using CTMC method, and the significance of different electron-electron correlations are discussed. A particular emphasis is put on the origin of the structure observed in the experimental angular-differential cross sections. We interpret the structure as Fraunhofer-type diffraction of the He^+ projectile de Broglie wave on the "aperture" formed due to the limited spatial region for the single-electron capture.

Atomic units (a.u.) will be used throughout unless otherwise indicated.

II. EXPERIMENT SETUP

The experiment was performed with a reaction microscope at the 320-kV platform for multidisciplinary research with highly charged ions at the Institute of Modern Physics, Lanzhou [46,58,59]. The working principles of the reaction microscope have been described in detail elsewhere [31,32,46]. The He^+ ions were produced in the 14.5-GHz electron cyclotron resonance and then accelerated to the desired energy. Two sets of adjustable slits upstream from the target chamber were used to collimate the beam to a size of about 1.0×1.0 mm^2 in the collision zone. Several sets of electrostatic deflectors immediately in front of the target zone were used to clean charge state impurities from the beam and to steer the beam to the target.

In the target chamber, the He^+ beam intersected with a well-localized He beam produced from a two-stage differentially pumped supersonic gas jet. The typical target density is estimated to be about 5×10^{11} atoms/cm^2 with a driving pressure of 4 bar. A homogeneous electrostatic field of

1.4 V/cm perpendicular to the incoming He^+ is applied in the target zone in order to extract the recoil ions from the interaction zone and guide the ions towards a position-sensitive detector. The extraction region is followed by a field-free drift tube. To reduce the influence of the finite size of the interaction area on the momentum resolution, we used one-dimensional time focusing geometry [60] where the length of the drift tube is twice the accelerating length. Specifically, in this work, the lengths of the tubes are 107.5 and 215.0 mm. An electrostatic deflector downstream from the target zone was used to separate the primary projectile beam from the He products. Finally, the primary projectile beam was collected with a Faraday cup, whereas the neutral He products were detected with a position-sensitive detector located about 1.5 m downstream from the target zone.

In the present experiment, the recoil ion He^+ was recorded in coincidence with the scattered projectile He. The momentum vector of the recoil ion could be reconstructed from the time of flight and the impact position on the detector. Note that the resolution of the momentum depends on the momentum itself and therefore the average values are provided here. The momentum resolution was estimated to be 0.03 a.u. in the x direction (electrostatic field direction) and 0.4 a.u. in the y direction (target beam direction) and z direction (projectile beam direction). More detailed information on resolution can be found in Ref. [61].

III. THEORETICAL METHOD

In this work, we developed a simulation code based on the dynamic-screening classical trajectory Monte Carlo (dCTMC) method developed by Montemayor and Schiwietz [62] to treat single-electron capture in the collision of slow He^+ ions with helium atoms. The CTMC method was proposed by Abrines and Percival [63,64] and has been extensively described in the past [65,66]. Hence, only a brief description is given here. The method is based on the numerical integration of the Hamilton equations of a classical four-body system which includes the incident ion, target nucleus, and two electrons initially bound to the target nucleus.

The initial states of the target electrons are obtained from a microcanonical phase-space distribution which was developed by Reinhold and Falcon [65] and has been widely employed in various versions of CTMC calculations [67,68]. Note that the target has two active electrons which have same initial position and momentum distributions. Model potentials developed by Green *et al.* [69] based on Hartree–Fork calculations, and later on generalized by Szydlik *et al.* [70] and Garvey *et al.* [71], are used to describe the interaction between the active electrons and the projectile ion, which reads [72]

$$V_p(r) = -[Z_p - (Z_p - 1)S(r)]/r, \qquad (1)$$

with

$$S(r) = 1 - \{(\eta/\xi)[\exp(\xi r) - 1] + 1\}^{-1}, \qquad (2)$$

where $Z_p = 2$ is the nuclear charge of the projectile. For the He^+ projectile, the parameters $\eta = 1.77$ and $\xi = 2.625$ were used [71]. Such a potential is also used to represent the interaction between the projectile ion and the target nucleus.

For the interactions between the two active electrons and the target nucleus in the initial channel, we adopt the screening potential developed by Montemayor and Schiwietz [62] in which the electron-electron interaction is partially taken into account by means of a dynamic screening of the target nucleus as seen by each of the two active electrons. The interactions are given by

$$
\begin{aligned}
&V_{te}(|\vec{r}_t - \vec{r}_1|, |\vec{r}_t - \vec{r}_2|, \zeta_1, \zeta_2) \\
&= -\frac{Z_t}{|\vec{r}_t - \vec{r}_1|} + \frac{1 - (1 + \zeta_2|\vec{r}_t - \vec{r}_1|)\exp(-2\zeta_2|\vec{r}_t - \vec{r}_1|)}{|\vec{r}_t - \vec{r}_1|} \\
&\quad - \frac{Z_t}{|\vec{r}_t - \vec{r}_2|} + \frac{1 - (1 + \zeta_1|\vec{r}_t - \vec{r}_2|)\exp(-2\zeta_1|\vec{r}_t - \vec{r}_2|)}{|\vec{r}_t - \vec{r}_2|}
\end{aligned}
\tag{3}
$$

with

$$
\zeta_j(t) = \begin{cases}
0, & I_j \leqslant 0 \\
(\zeta_{1s}/I_{1s})I_j(t), & 0 < I_j < I_{1s} \\
\zeta_{1s}, & I_{1s} \leqslant I_j,
\end{cases}
\tag{4}
$$

where $\vec{r}_t$, $\vec{r}_1$, and $\vec{r}_2$ is the position vector of the target nucleus, the first electron, and the second electron, respectively. Z_t is the nuclear charge of the target, I_j is the binding energy of electron j which is given by the net energy of electron j in the helium atom minus its kinetic energy. I_{1s} is the ionization energy of an electron in the $1s$ state of helium. The constant ζ_{1s} has the value $\zeta_{1s} = 1.687\,50$ [62].

In the final channel, if the total energy of either electron relative to the He nucleus becomes positive, the corresponding screening effect generated by this electron vanishes [see Eq. (3)]. Then the explicit $1/r_{12}$ interaction between the two electrons was turned on exponentially to enable electron-electron scattering but avoiding autoionization [25,28]. The switch function is defined by $1 - e^{-\gamma(t - t_0)}$ where γ is a constant and t_0 is the time at which the electron proceeds in a continuum state of the target [28]. In our case the calculated results are somewhat insensitive to the value of γ and $\gamma = 0.5$ a.u is used in the calculations. Therefore, both the dynamic and the static electron-electron correlations were taken into account in the theory.

The coupled Hamiltonian equations of motion are numerically solved by means of the Runge–Kutta–Gill method. In favor of the rapid development of the computer technology, it is not uncommon that the equations be solved for up to 10^7 trajectories to reduce statistical errors. To obtain good statistics for the determination of the state-selective cross sections we solved 10^5–10^7 individual trajectories at each collision energy in the present work. At the end of the trajectories, the different channels can be distinguished by performing a standard exit test [73] based on the calculations of the electron energy relative to the target ion and the projectile ion. For each trajectory that results in electron capture, the momenta of the four bodies and the corresponding impact parameter are saved.

In most of the previous CTMC calculations, each final state is assigned to specific n-quantal levels by using a semiquantal binning procedure derived by MacKellar and Becker [74]. However, the projectile in this work is dressed rather than bare and thus such a general binning procedure does not apply. The quantal defect due to the screening effect originated from
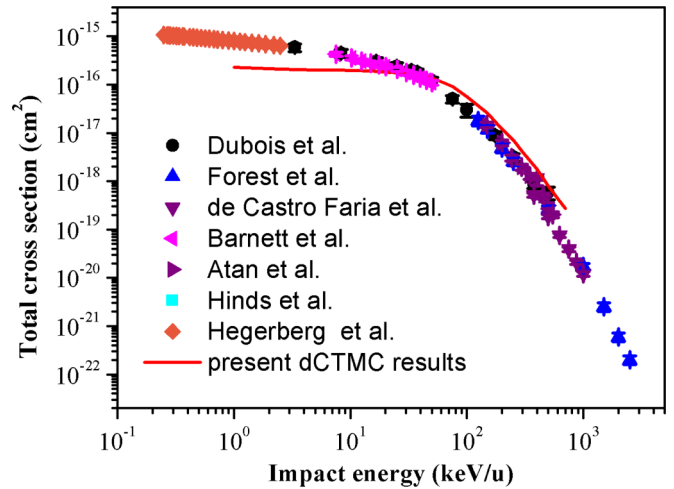
FIG. 1. Total cross sections for single capture in He$^+$ + He collisions. Experimental data: ● DuBois *et al.* [8]; ▲ Forest *et al.* [49]; ▼ de Castro Faria *et al.* [50]; ◄ Barnett *et al.* [51]; ► Atan *et al.* [52]; ■ Hinds *et al.* [53]; ◆ Hegerberg *et al.* [54]. Solid line is present dCTMC calculation.

the initially bound electron in the dressed projectile has to be taken into account in the binning procedure. Therefore, in this work the binning method with a well-defined effective charge suggested by Schultz *et al.* [75] is applied to calculate the n-state-selective capture cross sections. In this effective charge method, an effective charge $Q(U)$ is introduced instead of the projectile ionic charge q to represent the effective charge seen by the captured electron according to its binding energy. This method extends the applicability and reliability of the widely used Becker–Mackellar method for dressed projectile ion.

As a check of our dCTMC computer code, we performed test calculations for the single ionization, single capture and double ionization in collisions of protons with He atoms. Our results agree well with those of Montemayor and Schiwietz [62] and Meng *et al.* [76].

In this study, the dCTMC code is applied to treat the single electron capture in the collision of slow He$^+$ ions with helium atoms. Both differential and total cross sections were calculated. The calculated total cross sections are shown in Fig. 1 and compared with reported measurements [8,49–54]. As can be seen from Fig. 1, the present dCTMC results are in very good agreement with the experimental results in intermediate- and high-velocity collisions, i.e., for the impact energies larger than 10 keV/u. In contrast, in slow He$^+$ + He collisions, the present dCTMC results underestimate the experimental data. This could be due to the lack of angular correlation between the electrons and the quantum-mechanical tunneling effect in the dCTMC method. Such angular correlation and the tunneling effect are expected to play important roles in the low-impact-energy range because the collision partners have a longer time to interact with each other. In spite of the discrepancy, dCTMC gives an overall good description of the many-active-electron process. In the following sections, we employ the dCTMC method to calculate the differential cross sections and to explore the dynamics behind the process.
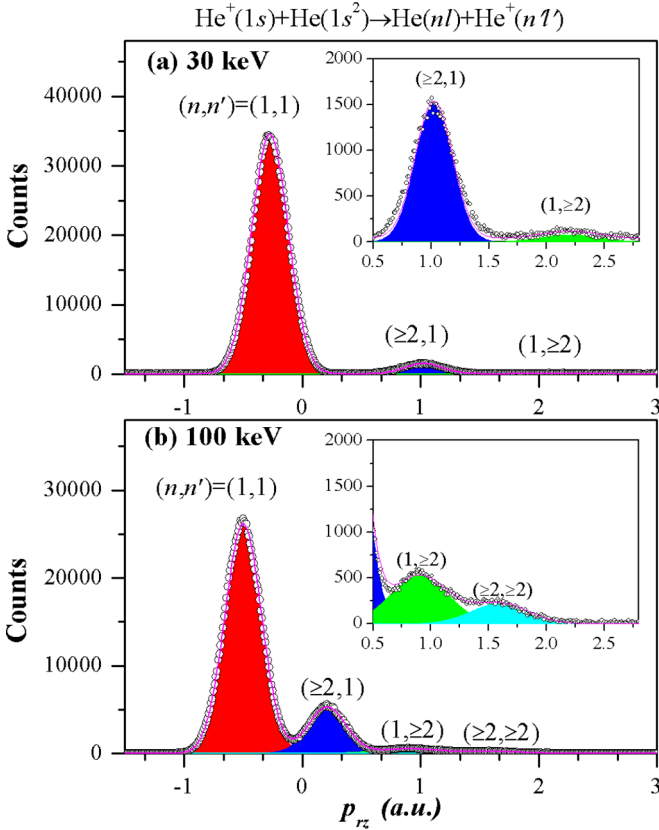
FIG. 2. Longitudinal recoil ion momentum for single capture in He$^+$ + He collisions at (a) 30 keV and (b) 100 keV impact energy.

FIG. 3. The absolute state-selective cross sections as a function of impact energy for single-electron capture from He in collisions with He$^+$. Solid symbols: present measurements; solid lines: present dCTMC results; dash lines: present dCTMC-c results; dash dot lines: present CTMC-s results (see text).

IV. RESULTS AND DISCUSSION

A. State-selective electron-capture cross sections

The longitudinal recoil ion momentum distributions are shown in Fig. 2. The absolute scale of the momentum is calibrated by using the well-defined single-capture process in He^{2+} + He collisions. The different peaks correspond to different final states indicated by (n,n'). In this notation, n denotes the individual quantum number of the captured electron while n' denotes that of the electron which remains bound to the target. At the lower impact energy of 30 keV, the spectrum indicates that the ground-state transfer ($n = 1$, $n' = 1$) is overwhelmingly dominant over the other processes, in agreement with the consideration of "energy matching." This is a general feature in symmetric ion-atom charge-transfer process as the ground-state transfer for He$^+$ + He collision is a resonant charge-transfer process in which the binding-energy difference before and after the reaction is 0. Besides the dominant reaction channel, the contributions from the excited-state transfer ($n \geqslant 2$, $n' = 1$) can also be identified. The transfer excitation processes ($n = 1$, $n' \geqslant 2$) in which the electron is captured to the ground state of the projectile accompanied by excitation of the ionized target He$^+$ have only a negligible contribution to the total cross sections.

As the projectile impact energy increased to 100 keV, the ground-state transfer remains dominant. However, the excited-state transfer and transfer excitation become relatively important compared with the 30-keV case. In addition, other

transfer excitation channels involving the excitation of the projectile ($n \geqslant 2$, $n' \geqslant 2$) are found to open, as shown in the inset of Fig. 2(b). This contribution, which is much smaller than the other contributions mentioned above, is negligible within experimental error in the 30-keV case.

To extract the state-selective contributions the experimental results are fit by the Gaussian function. We show the state-selective cross sections as a function of the impact energy in Fig. 3. Note that, in order to obtain a direct comparison with the calculations, these cross sections were determined by normalization to the total cross sections from Ref. [77], which have an uncertainty of 20%. In the present data analysis, errors from normalization, instruments, fittings, and statistics were considered. For 100-keV impact energy, the contributions of the transfer excitation with or without excitation of the projectile are added up. The present experimental data are contrasted with calculations obtained by using the dCTMC method, as is shown in Fig. 3 by solid lines. The present dCTMC calculations cover a much larger energy range in contrast with the experiment.

For the differential cross sections at 100-keV impact energy, a very good agreement is found between the calculations and the experimental results. Nevertheless, for low impact energy, such as 30 keV in this case, the dCTMC results tend to slightly underestimate the contribution of the ground-state transfer process and overestimate the contribution of the transfer excitation process. This might be due to the lack of angular correlation between the electrons and the quantum-mechanical tunneling effect in the dCTMC method as mentioned above with regard to Fig. 1.

In spite of the discrepancy at low impact energies, a better agreement is expected at higher impact energy since the dCTMC provides an overall very good description of the total cross sections at large impact energies, as indicated in Fig. 1. Indeed, as the impact energy is increased, the dCTMC calculations predict a decrease of the cross sections of excited-

state transfer and transfer excitation at impact energies larger than 150 keV, in accordance with the tendency in intermediate- and high-impact-energy ion-atom collisions [14,46]. However, more experimental differential data are needed for comparison.

Concerning the relative contributions of the different channels, the present dCTMC results showed that the ground-state transfer is dominant in the whole energy range but tend to decrease with the increase of impact energy. By contrast, the relative contributions of excited-state transfer and transfer excitation gradually increase over much of the energy range. The increasing importance of transfer excitation could probably be attributed to the decreasing range of the effective impact parameter in higher-energy collisions, which may increase the chance of target excitation.

Furthermore, to reveal the roles played by different electron-electron correlation effects, we also performed calculations by using two other more basic CTMC methods. The first one is the common CTMC within the independent-electron model [65] in which the initial dynamic screening effect related to the radial electron-electron correlations is not taken into account. In this method, the interaction between the frozen He^+ target core and the electron is represented by the model potential used in Ref. [65], while the projectile-electron and projectile-He^+ core interactions are described by the model potential as shown in Eq. (1). In the following, such a method is termed "CTMC-s." The second CTMC method is similar to the above dCTMC method, but without explicit inclusion of the $1/r_{12}$ interaction between the two active electrons in the final channel which is referred to as dCTMC-c. In general, the comparisons of the various calculations may shed some light on the importance of the electron-electron correlations, as demonstrated by a number of previous studies. To facilitate comparisons, the various results are shown in Fig. 3 together with the experimental data and the former dCTMC results. It was found that the different CTMC results show overall agreement with each other.

For ground-state transfer process the different CTMC calculations present almost identical results in the whole energy region, which suggests that these electron-electron correlations may play negligible roles in the ground-state transfer process.

For the excited-state transfer and transfer excitation, the three versions of CTMC predict similar cross sections both in behavior and magnitude in the high-energy range. However, there exists differences between the results for these two nonresonant processes.

On the one hand, for both excited-state transfer and transfer excitation, the dCTMC-c (dash lines) predicts slightly smaller cross sections than those of dCTMC at the impact energies smaller than about 100 keV. This indicates that the explicit electron-electron correlations during the collision may play a minor role in these processes, especially in the low-energy region.

On the other hand, the CTMC-s (dash dot lines) predicts smaller cross sections for excited-state transfer processes at impact energies larger than about 100 keV, while it predicts larger cross sections at impact energies smaller than about 50 keV. Note that, for excited-state transfer processes, CTMC-s demonstrates a similar agreement with the experiment in comparison with the other theoretical calculations, although

it predicts relatively larger cross sections around 30 keV. For transfer excitation processes, however, the CTMC-s method considerably deviates from the measurement and other calculations in the energy range smaller than about 300 keV. This suggests that the initial radial correlation originated from the dynamic screening effects may contribute to the single-electron capture process, especially for the process involving the excitation of the target electron.

B. Angular-differential cross sections

In Fig. 4 we show the projectile angular distributions for ground-state transfer in 30- and 100-keV He^+ + He single-capture process. The angular distributions display an oscillatory structure for both the impact energies. In Fig. 4 we also show the dCTMC results. As expected, the classical calculations are inadequate to reproduce the experimental data, although the widths are roughly same. Therefore, some other effects must be important in this process.

In the past, various mechanisms were proposed to interpret the observed oscillatory structure in the low- and intermediate-energy ranges, e.g., interference between the gerade and ungerade scattering amplitudes [78], kinematical effects due to the projectile-electron scattering [79], and Fraunhofer diffraction of the matter wave of the projectile [42,44]. It is known that the molecular states interference occurs at low
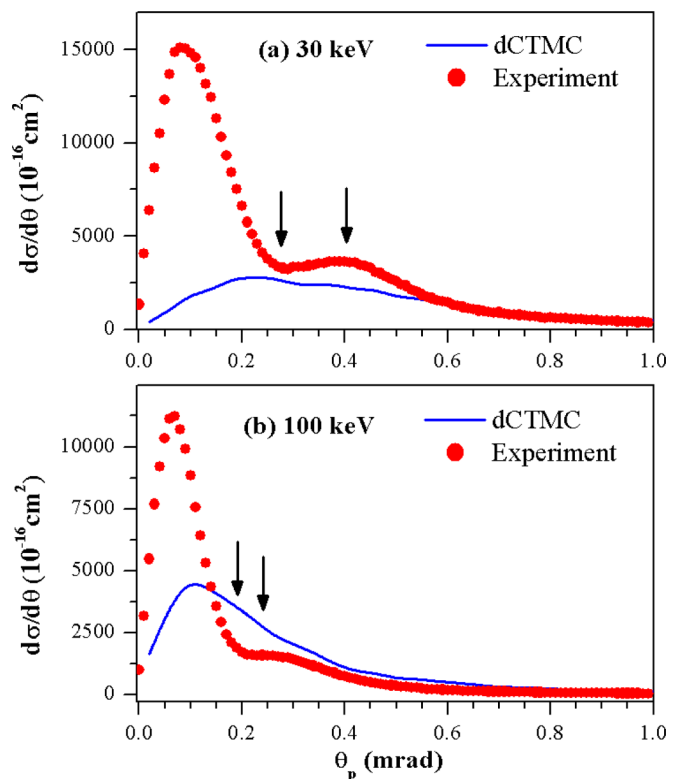
FIG. 4. The projectile angular-differential cross sections for ground-state transfer in He^+ + He collisions at (a) 30-keV and (b) 100-keV impact energy. Open circles: present measurements; solid lines: present dCTMC results. The arrows indicate the positions of the first dark and first bright fringes expected from Fraunhofer-type diffraction theory.

energy [78,80] and gives rise to oscillatory structure at larger scattering angles. Thus this mechanism could become less important in the present case since low impact energy such as 30 keV in our work is at the upper edge of the energy region in which the molecular picture works. It can be estimated that the kinematical electron capture could lead to a maxima at the characteristic scattering angle of 0.14 mrad; by contrast, the oscillations in our experimental distributions do not show any such signature related to the kinematical effect. Thus the second mechanism can also be neglected.

Due to the fact that the single capture can only take place in a limited spatial region close to the target, the oscillatory structures may be understood in a Fraunhofer diffraction picture since the single-capture process of charged ions on atoms is closely analogous to Fraunhofer diffraction of light [44].

On the grounds of Fraunhofer-type diffraction theory [81], the first dark and the first bright fringes are located at $0.61\lambda/\rho$ and $0.819\lambda/\rho$, respectively, where ρ is the aperture radius and λ the wavelength of incident wave. Since the wavelength of the atomic matter wave is well known from the de Broglie relationship, a reliable estimate of the aperture radius is necessary to make a quantitative comparison with the experimental angular positions of the maxima and minima.

In the single-capture process the aperture radius is represented by the effective impact parameter range in which the single-capture process may take place. By using the dCTMC method we can obtain the impact-parameter dependence of the single-capture probabilities. The calculated ground-state transfer probabilities as a function of the impact parameter are shown in Fig. 5. We observe a step-like distribution which is analogous to a pupil function in optics, and the widths are almost same for both the impact energies. A close inspection indicates that the corresponding impact parameter range becomes slightly narrower as the impact energy increases. Similar calculations for electron capture by various charged ions from helium atoms show that the impact parameter range becomes smaller as the impact energy increases [66]. It is understandable since the collision partners interact with each other for an increasing period of time as
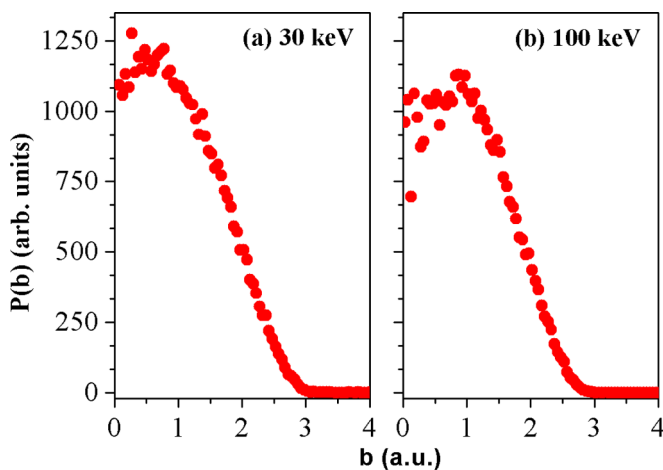
FIG. 5. The calculated ground-state transfer probabilities in He$^+$ + He collisions at (a) 30-keV and (b) 100-keV impact energy.

the impact energy decreases and thus the effective interaction region extends. This result supports the assumption we made in Sec. IV A with regard to the state-selective cross sections.

For the present impact energies of 30 and 100 keV, the wavelength of the atomic matter wave of the projectile is 0.001 56 a.u. and 0.000 86 a.u., and the calculated maximum impact parameter (e.g., equivalent to the aperture radius) is approximately 3.0 a.u. and 2.9 a.u., respectively. Inserting the wavelength and the calculated impact parameter range into the above relations yields the expected positions of the first dark and the first bright fringes. In Fig. 4 the positions of the first dark and first bright fringes expected from the Fraunhofer-type diffraction theory are indicated by arrows. The strikingly good agreement of the positions of arrows and the experimental results suggests that the oscillation structure appearing in the angle distributions originates from atomic-size Fraunhofer-type diffraction.

V. CONCLUSION

By using the reaction microscopes we have investigated the single capture in He$^+$ + He collisions at impact energies of 30 and 100 keV. The state-selective cross sections and the projectile angular-differential cross sections have been extracted from the measurements. It was found that the ground-state transfer process is dominant over excited-state transfer and transfer excitation processes. Furthermore, by using the dCTMC method we calculated the state-selective cross sections. Very good agreement is found for 100-keV impact energy, while there is an apparent deviation between experiment and theory at 30-keV impact energy. This could probably be attributed to the poor performance of CTMC method in the low-energy range, which originates from the lack of angular correlation and the quantum-mechanical tunneling effect in the method. Moreover, the comparisons of the various CTMC calculations with experimental data shed more light onto the roles played by the different electron-electron correlation effects.

In the projectile angular-differential cross sections, we observed a similar oscillation structure for the two impact energies. The structure is explained in terms of Fraunhofer-type diffraction of the He$^+$ projectile de Broglie wave on "aperture" formed due to the limited spatial region in which the single-electron capture processes take place. Based on Fraunhofer-type diffraction theory, the characteristics of the structure agree well with the quantitative estimate using the impact parameter range obtained from dCTMC calculations. We may conclude that the characteristic oscillation structure was caused by matter-wave Fraunhofer-type diffraction.

[1] R. C. Isler, Phys. Scr. **35**, 650 (1987).

[2] R. C. Isler, Plasma Phys. Control. Fusion **36**, 171 (1994).

[3] T. Cravens, Science **296**, 1042 (2002).

[4] P. Beiersdorfer, K. Boyce, G. Brown, H. Chen, S. Kahn, R. Kelley, M. May, R. Olson, F. Porter, C. Stahle, and W. Tillotson, Science **300**, 1558 (2003).

[5] *Many-Particle Quantum Dynamics in Atomic and Molecular Fragmentation*, Springer Series on Atomic, Optical, and Plasma Physics, edited by J. Ullrich and V. Shevelko (Springer, Berlin, 2003), Vol. 35.

[6] M. B. Shah, P. McCallion, and H. B. Gilbody, J. Phys. B: At., Mol. Opt. Phys. **22**, 3037 (1989).

[7] M. B. Shah and H. B. Gilbody, J. Phys. B: At. Mol. Phys. **18**, 899 (1985).

[8] R. D. DuBois, Phys. Rev. A **39**, 4440 (1989).

[9] K. Okuno, H. Tawara, T. Iwai, Y. Kaneko, M. Kimura, N. Kobayashi, A. Matsumoto, S. Ohtani, S. Takagi, and S. Tsurubuchi, Phys. Rev. A **28**, 127 (1983).

[10] C. Schmeissner, C. L. Cocke, R. Mann, and W. Meyerhof, Phys. Rev. A **30**, 1661 (1984).

[11] B. A. Huber and H. J. Kahlert, J. Phys. B: At. Mol. Phys. **16**, 4655 (1983).

[12] T. Hayakawa, R. A. Lomsadze, C. Verzani, H. Watanabe, H. Tanuma, B. D. DePaola, and N. Kobayashi, Phys. Scr. **2001**, 322 (2001).

[13] S. Bliman, R. Bruch, M. Cornille, A. Langereis, and J. Nordgren, Phys. Rev. A **66**, 052707 (2002).

[14] H.-K. Kim, M. S. Schöffler, S. Houamer, O. Chuluunbaatar, J. N. Titze, L. P. H. Schmidt, T. Jahnke, H. Schmidt-Böcking, A. Galstyan, Y. V. Popov, and R. Dörner, Phys. Rev. A **85**, 022707 (2012).

[15] W. Fritsch and C. Lin, Phys. Rep. **202**, 1 (1991).

[16] W. Fritsch and C. D. Lin, Phys. Rev. A **54**, 4931 (1996).

[17] J. P. Hansen, A. Dubois, and S. E. Nielsen, Phys. Rev. A **45**, 184 (1992).

[18] R. J. Allan, C. Courbin, P. Salas, and P. Wahnon, J. Phys. B: At., Mol. Opt. Phys. **23**, L461 (1990).

[19] N. Toshima, Phys. Rev. A **59**, 1981 (1999).

[20] T. G. Winter, Phys. Rev. A **87**, 032704 (2013).

[21] R. Dörner, V. Mergel, R. Ali, U. Buck, C. L. Cocke, K. Froschauer, O. Jagutzki, S. Lencinas, W. E. Meyerhof, S. Nüttgens, R. E. Olson, H. Schmidt-Böcking, L. Spielberger, K. Tökesi, J. Ullrich, M. Unverzagt, and W. Wu, Phys. Rev. Lett. **72**, 3166 (1994).

[22] A. Cassimi, S. Duponchel, X. Flechard, P. Jardin, P. Sortais, D. Hennecart, and R. E. Olson, Phys. Rev. Lett. **76**, 3679 (1996).

[23] R. Dörner, H. Khemliche, M. H. Prior, C. L. Cocke, J. A. Gary, R. E. Olson, V. Mergel, J. Ullrich, and H. Schmidt-Böcking, Phys. Rev. Lett. **77**, 4520 (1996).

[24] R. Moshammer, J. Ullrich, H. Kollmus, W. Schmitt, M. Unverzagt, O. Jagutzki, V. Mergel, H. Schmidt-Böcking, R. Mann, C. J. Woods, and R. E. Olson, Phys. Rev. Lett. **77**, 1242 (1996).

[25] V. Mergel, R. Dörner, M. Achler, K. Khayyat, S. Lencinas, J. Euler, O. Jagutzki, S. Nüttgens, M. Unverzagt, L. Spielberger, W. Wu, R. Ali, J. Ullrich, H. Cederquist, A. Salin, C. J. Wood, R. E. Olson, D. Belkić, C. L. Cocke, and H. Schmidt-Böcking, Phys. Rev. Lett. **79**, 387 (1997).

[26] H. Kollmus, R. Moshammer, R. E. Olson, S. Hagmann, M. Schulz, and J. Ullrich, Phys. Rev. Lett. **88**, 103202 (2002).

[27] R. E. Olson, T. J. Gay, H. G. Berry, E. B. Hale, and V. D. Irby, Phys. Rev. Lett. **59**, 36 (1987).

[28] M. Alessi, N. D. Cariatore, P. Focke, and S. Otranto, Phys. Rev. A **85**, 042704 (2012).

[29] M. Alessi, S. Otranto, and P. Focke, Phys. Rev. A **83**, 014701 (2011).

[30] *Atomic Processes in Basic and Applied Physics*, Springer Series on Atomic, Optical, and Plasma Physics, edited by H. T. Viacheslav Shevelko (Springer, Berlin, Heidelberg, 2012), Vol. 68.

[31] R. Dörner, V. Mergel, O. Jagutzki, L. Spielberger, J. Ullrich, R. Moshammer, and H. Schmidt-Böcking, Phys. Rep. **330**, 95 (2000).

[32] J. Ullrich, R. Moshammer, A. Dorn, R. Dörner, L. P. H. Schmidt, and H. Schmidt-Böcking, Rep. Prog. Phys. **66**, 1463 (2003).

[33] D. Fischer, B. Feuerstein, R. D. DuBois, R. Moshammer, J. R. C. Lopez-Urrutia, I. Draganic, H. Lorch, A. N. Perumal, and J. Ullrich, J. Phys. B **35**, 1369 (2002).

[34] C. Courbin, M. Machholm, I. Reiser, D. Dowek, and J. C. Houver, J. Phys. B: At., Mol. Opt. Phys. **31**, 2305 (1998).

[35] M. Machholm and C. Courbin, J. Phys. B: At., Mol. Opt. Phys. **27**, 4703 (1994).

[36] M. Machholm and C. Courbin, J. Phys. B: At., Mol. Opt. Phys. **29**, 1079 (1996).

[37] S. E. Nielsen, J. P. Hansen, and A. Dubois, J. Phys. B: At., Mol. Opt. Phys. **28**, 5295 (1995).

[38] J. W. Thomsen, I. Reiser, N. Andersen, J. C. Houver, J. Salgado, E. Sidky, A. Svensson, and D. Dowek, J. Phys. B: At., Mol. Opt. Phys. **29**, 5459 (1996).

[39] S. Grego, J. Salgado, J. W. Thomsen, M. Machholm, S. E. Nielsen, and N. Andersen, J. Phys. B: At., Mol. Opt. Phys. **31**, 3419 (1998).

[40] J. W. Thomsen, J. Salgado, N. Andersen, D. Dowek, A. Dubois, J. C. Houver, S. E. Nielsen, and A. Svensson, J. Phys. B: At., Mol. Opt. Phys. **32**, 5189 (1999).

[41] M. S. Schöffler, J. Titze, L. P. H. Schmidt, T. Jahnke, N. Neumann, O. Jagutzki, H. Schmidt-Böcking, R. Dörner, and I. Mančev, Phys. Rev. A **79**, 064701 (2009).

[42] S. Knoop, R. E. Olson, H. Ott, V. G. Hasan, R. Morgenstern, and R. Hoekstra, J. Phys. B: At., Mol. Opt. Phys. **38**, 1987 (2005).

[43] M. van der Poel, C. V. Nielsen, M.-A. Gearba, and N. Andersen, Phys. Rev. Lett. **87**, 123201 (2001).

[44] Q. Wang, X. Ma, X. L. Zhu, and S. F. Zhang, J. Phys. B: At., Mol. Opt. Phys. **45**, 025202 (2012).

[45] D. Fischer, M. Gudmundsson, Z. Berényi, N. Haag, H. A. B. Johansson, D. Misra, P. Reinhed, A. Källberg, A. Simonsson, K. Støchkel, H. Cederquist, and H. T. Schmidt, Phys. Rev. A **81**, 012714 (2010).

[46] D. L. Guo, X. Ma, S. F. Zhang, X. L. Zhu, W. T. Feng, R. T. Zhang, B. Li, H. P. Liu, S. C. Yan, P. J. Zhang, and Q. Wang, Phys. Rev. A **86**, 052707 (2012).

[47] M. S. Schöffler, H.-K. Kim, O. Chuluunbaatar, S. Houamer, A. G. Galstyan, J. N. Titze, T. Jahnke, L. P. H. Schmidt, H. Schmidt-Böcking, R. Dörner, Y. V. Popov, and A. A. Bulychev, Phys. Rev. A **89**, 032707 (2014).

[48] J. Bradley, S. F. C. O'Rourke, and D. S. F. Crothers, Phys. Rev. A **71**, 032706 (2005).

[49] J. L. Forest, J. A. Tanis, S. M. Ferguson, R. R. Haar, K. Lifrieri, and V. L. Plano, Phys. Rev. A **52**, 350 (1995).

[50] N. V. de Castro Faria, F. L. Freire, and A. G. de Pinho, Phys. Rev. A **37**, 280 (1988).

[51] C. F. Barnett and P. M. Stier, Phys. Rev. **109**, 385 (1958).

[52] H. Atan, W. Steckelmacher, and M. W. Lucas, J. Phys. B: At., Mol. Opt. Phys. **24**, 2559 (1991).

[53] E. A. Hinds and R. Novick, J. Phys. B: At. Mol. Phys. **11**, 2201 (1978).

[54] R. Hegerberg, T. Stefansson, and M. T. Elford, J. Phys. B: At. Mol. Phys. **11**, 133 (1978).

[55] I. Mančev, Phys. Rev. A **75**, 052716 (2007).

[56] A. Jain, R. Shingal, and T. J. M. Zouros, Phys. Rev. A **43**, 1621 (1991).

[57] M. Ourdane, H. Bachau, R. Gayet, and J. Hanssen, J. Phys. B: At., Mol. Opt. Phys. **32**, 2041 (1999).

[58] X. Ma, X. Zhu, H. Liu, B. Li, S. Zhang, S. Cao, W. Feng, and S. Xu, Sci. China, Ser. G: Phys., Mech. Astron. **51**, 755 (2008).

[59] X. Ma, R. T. Zhang, S. F. Zhang, X. L. Zhu, W. T. Feng, D. L. Guo, B. Li, H. P. Liu, C. Y. Li, J. G. Wang, S. C. Yan, P. J. Zhang, and Q. Wang, Phys. Rev. A **83**, 052707 (2011).

[60] W. C. Wiley and I. H. McLaren, Rev. Sci. Instrum. **26**, 1150 (1955).

[61] D. L. Guo, X. Ma, W. T. Feng, S. F. Zhang, and X. L. Zhu, Acta Phys. Sin. **60**, 113401 (2011).

[62] V. J. Montemayor and G. Schiwietz, Phys. Rev. A **40**, 6223 (1989).

[63] R. Abrines and I. C. Percival, Proc. Phys. Soc., London **88**, 861 (1966).

[64] R. Abrines and I. C. Percival, Proc. Phys. Soc., London **88**, 873 (1966).

[65] C. O. Reinhold and C. A. Falcón, Phys. Rev. A **33**, 3859 (1986).

[66] R. E. Olson and A. Salop, Phys. Rev. A **16**, 531 (1977).

[67] E. Lewartowski and C. Courbin, J. Phys. B: At., Mol. Opt. Phys. **26**, 3403 (1993).

[68] R. E. Olson, C. J. Wood, H. Schmidt-Böcking, R. Moshammer, and J. Ullrich, Phys. Rev. A **58**, 270 (1998).

[69] A. E. S. Green, D. L. Sellin, and A. S. Zachor, Phys. Rev. **184**, 1 (1969).

[70] P. P. Szydlik and A. E. S. Green, Phys. Rev. A **9**, 1885 (1974).

[71] R. H. Garvey, C. H. Jackman, and A. E. S. Green, Phys. Rev. A **12**, 1144 (1975).

[72] S. Otranto, R. E. Olson, and P. Beiersdorfer, Phys. Rev. A **73**, 022723 (2006).

[73] M. L. McKenzie and R. E. Olson, Phys. Rev. A **35**, 2863 (1987).

[74] R. L. Becker and A. D. MacKellar, J. Phys. B: At. Mol. Phys. **17**, 3923 (1984).

[75] D. R. Schultz, P. C. Stancil, and M. J. Rakovic, J. Phys. B: At., Mol. Opt. Phys. **34**, 2739 (2001).

[76] L. Meng, R. E. Olson, R. Dorner, J. Ullrich, and H. Schmidt-Bocking, J. Phys. B: At., Mol. Opt. Phys. **26**, 3387 (1993).

[77] *Atomic Data for Controlled Fusion Research*, edited by C. F. Barnett, J. A. Ray, E. Ricci, M. I. Wilker, E. W. McDaniel, E. W. Thomas, and H. B. Gilbody (Oak Ridge National Laboratory, Oak Ridge, 1990), Vol. 1.

[78] R. S. Gao, L. K. Johnson, D. A. Schafer, J. H. Newman, K. A. Smith, and R. F. Stebbings, Phys. Rev. A **38**, 2789 (1988).

[79] E. Horsdal, B. Jensen, and K. O. Nielsen, Phys. Rev. Lett. **57**, 1414 (1986).

[80] M. Barat, J. C. Brenot, and J. Pommier, J. Phys. B: At. Mol. Phys. **6**, L105 (1973).

[81] M. Born and E. Wolf, *Principles of Optics: Electromagnetic Theory of Propagation, Interference and Diffraction of Light* (Cambridge University Press, Cambridge, 2000).